Applied Physics Letters

RESEARCH ARTICLE | NOVEMBER 10 2025

Thermal transport mapping in twisted double bilayer graphene

Special Collection: Thermal Properties of Graphene and Carbon Materials – From Physics to Applications in Thermal Management

Roop Kumar Mech; Alessandra Canetta ; Yubin Huang; Sergio Gonzalez-Munoz ; Khushboo Agarwal ; Pauline de Crombrugghe; Yuanzhuo Hong ; Sambit Mohapatra ; Kenji Watanabe ; Takashi Taniguchi; Bernard Nysten ; Benoît Hackens ; Rebeca Ribeiro-Palau ; Oleg Kolosov ; Jean Spièce ; Pascal Gehring

Appl. Phys. Lett. 127, 192201 (2025)
https://doi.org/10.1063/5.0289373

AIP Publishing

Applied Physics Letters ARTICLE pubs.aip.org/aip/apl

Thermal transport mapping in twisted double bilayer graphene

Cite as: Appl. Phys. Lett. **127**, 192201 (2025); doi: 10.1063/5.0289373
Submitted: 7 July 2025 · Accepted: 24 October 2025 ·
Published Online: 10 November 2025

Roop Kumar Mech,[1] Alessandra Canetta,[1] Yubin Huang,[1] Sergio Gonzalez-Munoz,[2] Khushboo Agarwal,[2] Pauline de Crombrugghe,[1] Yuanzhuo Hong,[3] Sambit Mohapatra,[3] Kenji Watanabe,[4] Takashi Taniguchi,[5] Bernard Nysten,[1] Benoît Hackens,[1] Rebeca Ribeiro-Palau,[3] Oleg Kolosov,[2,a)] Jean Spièce,[1,b)] and Pascal Gehring[1,c)]

AFFILIATIONS

[1]IMCN, Université Catholique de Louvain (UCLouvain), 1348 Louvain-la-Neuve, Belgium
[2]Physics Department, Lancaster University, Lancaster, United Kingdom
[3]Université Paris-Saclay, CNRS, Centre de Nanosciences et de Nanotechnologies (C2N), 91120 Palaiseau, France
[4]Research Center for Electronic and Optical Materials, National Institute for Materials Science, 1-1 Namiki, Tsukuba 305-0044, Japan
[5]Research Center for Materials Nanoarchitectonics, National Institute for Materials Science, 1-1 Namiki, Tsukuba 305-0044, Japan

Note: This paper is part of the Special Topic, Thermal Properties of Graphene and Carbon Materials — From Physics to Applications in Thermal Management.
[a)]**Electronic mail:** o.kolosov@lancaster.ac.uk
[b)]**Author to whom correspondence should be addressed:** jean.spiece@uclouvain.be
[c)]**Electronic mail:** pascal.gehring@uclouvain.be

ABSTRACT

Two-dimensional (2D) materials have attracted significant interest due to their tunable physical properties when stacked into homo- and heterostructures. Twisting adjacent layers introduces moiré patterns that strongly influence the material's electronic and thermal behavior. In twisted graphene systems, the twist angle critically alters phonon transport, leading to reduced thermal conductivity compared to Bernal-stacked configurations. However, experimental investigations into thermal transport in twisted structures remain limited. Here, we study the local thermal properties of low-angle ($< 1°$) twisted double bilayer graphene using scanning thermal microscopy. We find an increase in thermal resistance of $0.3 \pm 0.1 \times 10^6$ KW^{-1} compared to untwisted bilayers, attributed to changes in both intrinsic thermal conductivity and the tip–sample interface. Analytical modeling shows that such variations may be attributed to intrinsic conductivity changes or modifications of the tip–sample interface resistance, or a combination of both. Our study highlights how twist alters the overall thermal resistance network in graphene heterostructures, providing direct nanoscale evidence that moiré engineering impacts multiple pathways of heat dissipation. These insights advance understanding of thermal transport in twisted 2D systems and open avenues for thermal management in twistronic devices.

In recent years, two-dimensional (2D) materials have gained increasing attention. The atomic layers in these materials are held together by weak van der Waals forces, making them easy to cleave and stack into new heterostructures.[1] Stacking different 2D layers can result in artificial systems with novel physical properties.[2–4] Moreover, by twisting the layers with respect to each other, the periodicity of the resulting lattice changes, forming a so-called moiré pattern.[5] This twist angle becomes a crucial parameter for tuning the band structure[6] and the lattice symmetry of the new material.[7,8] At small twist angles,[9] the mismatch between layers leads to atomic reconstruction, favoring energetically stable stacking configurations. This results in discrete stacking domains and domain walls,[10] which are predicted to significantly affect the local thermal properties of twisted 2D systems.

The thermal conductivity of graphene has been reported to vary with the twist angle between its layers. Bernal-stacked (AB) graphene exhibits the highest thermal conductivity. Introducing a twist reduces this property: Li *et al.*[11] measured a 25% decrease at 34°, while Han *et al.*[12] observed a 15% decrease at 2°, both using optothermal Raman spectroscopy. These reductions are attributed to changes in low-frequency phonon transport and are supported by molecular dynamics simulations. Other studies[13–16] confirm that both in-plane and cross-plane thermal conductivities decrease as the twist angle increases.

These works suggest that twisting can influence phonon transport, although the magnitude of conductivity suppression depends strongly on the angle range and modeling assumptions. More recently, Feng *et al.*[17] reported a pronounced twist-angle dependence of bilayer graphene thermal conductivity, and Ouyang *et al.*[18] demonstrated controllable thermal transport at twisted graphene/hBN interfaces, further highlighting the role of interlayer orientation in heat conduction.

Despite its importance for device performance and stability, thermal transport in twisted graphene structures remains poorly explored experimentally. A quantitative understanding of how twist affects heat dissipation in graphene could lead to angle-engineered thermal interfaces and optimized thermal management in twistronic devices. However, experimental confirmation of these predictions is still lacking.

Here, we investigate the local thermal properties of twisted double bilayer graphene (TDBG) using scanning thermal microscopy (SThM). We observe an increase in the thermal resistance of TDBG by $0.3 \pm 0.1 \times 10^6$ KW^{-1} compared to untwisted double bilayer graphene. Analytical modeling indicates that such a change may originate from both intrinsic transport (e.g., thermal conductivity variations) and interfacial effects (e.g., tip–sample resistance), or a combination of both. Thus, our analysis highlights that twist modifies the overall thermal resistance network rather than a single mechanism alone.

Twisted double bilayer graphene consists of two AB-stacked bilayers placed on a 40 nm hexagonal boron nitride (hBN) substrate. A scheme of the full structure is shown in Fig. 1(a). When stacked, a small twist angle θ ($< 1°$) is introduced between the bilayers, forming a moiré pattern of ABAB and ABCA domains, while suppressing the less stable ABBC regions.[10,19] The TDBG was fabricated using a dry transfer method with a polycarbonate (PC) film (10% concentration) supported by a polydimethylsiloxane bubble stamp. Two halves of a bilayer graphene, precut using an atomic force microscope,[20] were picked up sequentially with a relative twist angle of less than 1°. The final stack was transferred onto a hBN flake at room temperature without melting the PC,[21] minimizing contamination during the process.

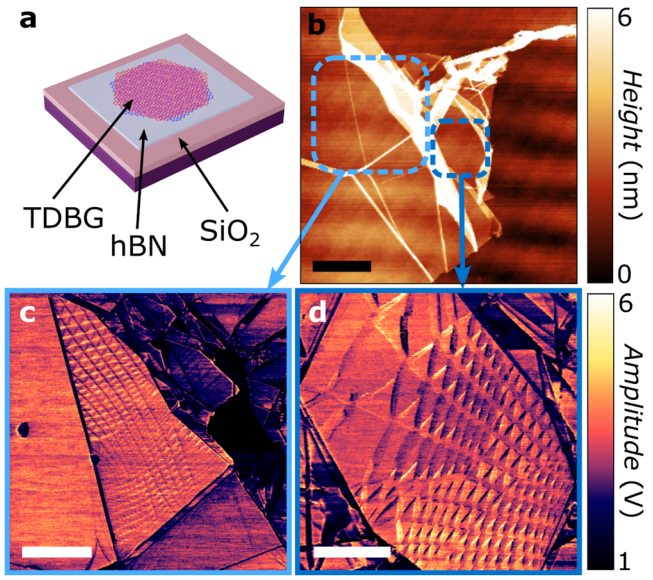

FIG. 1. (a) Scheme of the sample structure consisting of a hBN flake acting as substrate on which two graphene bilayers where stacked at a small angle. The whole 2D stack is resting on a 300 nm SiO_2 on Si wafer. (b) Topography map of the sample with the two regions showing large moiré patterns (highlighted by the dashed squares). Scale bar is 1 μm. (c) PFM small scale image of the first region in (b). Scale bar is 250 nm (d) PFM image of the other moiré region. Scale is 100 nm.

The moiré wavelength λ_m depends on the twist angle and is given by $\lambda_m = (a/2)/\sin(\theta/2)$, where a is the graphene lattice constant.[22] Using piezoresponse force microscopy (PFM), we identified two regions with large moiré wavelengths [Fig. 1(b)]. PFM is a useful tool to characterize twisted 2D systems due to their piezoelectric or flexoelectric responses.[23] In our PFM setup, an AC bias at the contact resonance frequency is applied between an electrically conductive atomic force microscopy (AFM) tip and the sample, generating a vertical electric field.[24,25] This field induces piezoelectric strain, which is detected through the AFM lever's torsion or deflection.

Figures 1(c) and 1(d) show PFM maps of the two regions. From these maps, we estimate effective twist angles between 0.07° and 0.15°. Both regions display stretched triangular domains, which may indicate the presence of local strain or pinning at specific stacking sites.[26]

To investigate thermal transport in our 2D system, we use scanning thermal microscopy, as described in previous studies.[27,28] SThM is a powerful technique that enables nanoscale mapping of heat dissipation in low-dimensional materials. Its operation is based on a sharp, microfabricated cantilever that functions both as a heater and a temperature sensor. The probe is raster-scanned across the sample surface using standard atomic force microscopy (AFM) feedback to control the tip–sample interaction.

Measurements were conducted under high vacuum conditions (10^{-6} Torr) using a sharp probe, ensuring accurate thermal mapping without interference from air or water meniscus.[27,28] We used commercially available doped silicon probes (Anasys Instruments, AN-300), which have a geometry similar to standard AFM probes but with a cantilever composed of two highly doped, electrically conductive legs. These probes form part of a Wheatstone bridge circuit used to detect small changes in electrical resistance. A DC or AC voltage applied to the bridge heats the probe to a few tens of kelvin above room temperature. The output signal is amplified and calibrated to extract the probe temperature. Calibration details of both the thermal signal and probe resistance vs temperature can be found elsewhere.[27]

Figure 2(a) illustrates the working principle of SThM and its corresponding thermal resistance model. When the probe contacts a low-conductivity material, less heat flows into the sample, causing the probe temperature to rise. This temperature change alters the electrical resistance of the probe, which is detected via the bridge circuit. Under ambient conditions, the relation between the contact and non-contact voltages can be written as[27,28]

$$\frac{V_{nc} - V_c}{V_{nc}} = \frac{R_p}{R_p + R_X}, \tag{1}$$

where V_{nc} and V_c are the measured voltages with the probe out of contact and in contact with the sample, respectively. R_p is the thermal resistance of the probe, and R_X is the thermal resistance of the sample.

As shown later in Fig. 2(a), the total measured thermal resistance R_X consists of three components in series,[27,28]

$$R_X = R_{tip} + R_{int} + R_{spr}, \tag{2}$$

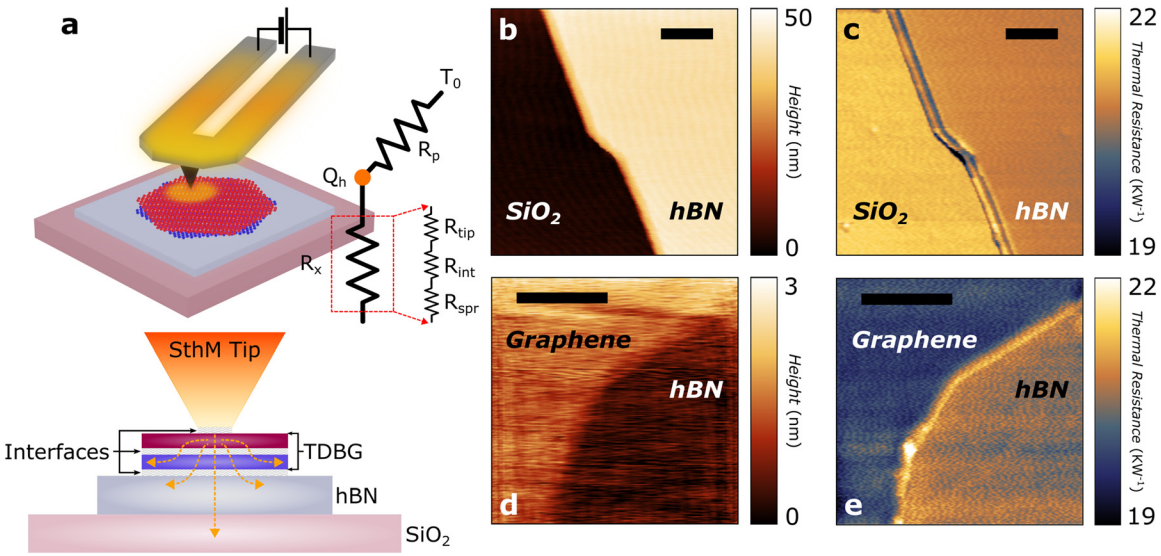

FIG. 2. (a) Schematic representation of the SThM probe and tip–sample system along with thermal resistances network. (b), (c) Topography and thermal resistance maps of the hBN flake on the silicon oxide substrate. (d) and (e) Topography and thermal resistance map of the step between hBN and 4 layers graphene. Lateral scale bars are 200 nm. Topography images and thermal resistance maps are in nm and KW^{-1}, respectively.

where R_{tip} is the thermal resistance of the conical tip, R_{int} is the tip–sample interface resistance, and R_{spr} is the sample's thermal spreading resistance. Proper interpretation of R_X requires separating and analyzing each component.

Figures 2(b) and 2(c) show topography and thermal resistance maps across a step between a silicon oxide (SiO_x) substrate and a 40 nm thick hBN flake. Due to hBN's high thermal conductivity, its measured thermal resistance is lower than that of SiO_x. However, it is important to note that the apparent thermal resistance includes various contributions and artifacts, such as those from the tip–sample interface, surface properties, and topography.[29]

Figures 2(d) and 2(e) show a similar measurement across a boundary between hBN and a four-layer graphene region on hBN. When the probe transitions from hBN to graphene, we observe a clear drop in thermal resistance of $1 \pm 0.2 \times 10^6$ KW^{-1}. While the difference in thermal conductivities—and therefore spreading resistances—between hBN and graphene may contribute to this contrast, it is not enough to fully account for the observed change. Since both materials are atomically flat and have high thermal conductivities, the main contribution must arise from variations in the tip–sample interface resistance.

The thermal interface resistance is given by $R_{int} = \frac{r_{int}^p}{\pi a^2}$, where r_{int}^p is the thermal interface resistivity, and a is the contact radius. To assess the lateral resolution of our SThM measurements, we analyzed line profiles across the hBN–graphene boundary (see the supplementary material, Part I). The apparent width of the transition in the thermal resistance signal was fitted with a step function convolved with a Gaussian point-spread function. From the extracted FWHM, we determine a thermal contact radius of 30 ± 5 nm. Using this and the observed thermal resistance drop, we calculate a change in interface resistivity of about $5 \pm 3\%$. This result confirms the high sensitivity of SThM to small variations in local heat transport. As we will show next, this sensitivity enables us to map thermal resistance differences between twisted graphene domains.

Figure 3(a) shows a scanning thermal microscopy image of the first twisted graphene region. The scan was taken across the boundary between the twisted and non-twisted areas to allow direct comparison of the thermal signal. As seen in the image, the thermal resistance increases in the twisted area by $\Delta R_X = 0.3 \pm 0.1 \times 10^6$ KW^{-1}. Topography and friction images reveal no visible differences between the two regions, confirming that the observed thermal contrast is not related to surface morphology or frictional properties.

A line profile extracted from the SThM image is shown in Fig. 3(b), along with a simultaneously acquired topography profile. A clear step in thermal resistance is visible at the twisted–non-twisted boundary, while no notable change is observed in the topography, aside from a slight graphene ripple marking the interface.

Next, we analyze the relative contributions of thermal interface resistance (R_{int}) and thermal spreading resistance (R_{spr}) to the observed change in ΔR_X.

We note that our experimental dataset focuses on a narrow range of small twist angles ($\sim 0.07\text{deg} \cup 0.15\text{deg}$). While this allows us to directly resolve thermal resistance changes across well-defined moiré domains, a systematic exploration over a broader twist-angle range would be required to fully establish the dependence of thermal resistance on twist angle. To further verify reproducibility, we performed additional measurements on two independent twisted–untwisted regions (supplementary material, Figs. 2 and 3). In both cases, we observe the same resistance contrast, confirming that the effect is robust across different sample locations.

Let R_X^0 and R_X^t denote the measured thermal resistances in the non-twisted and twisted regions, respectively. From Eq. (2), and assuming the tip resistance R_{tip} remains constant (as it is determined by the fixed probe geometry and apex size), the difference in thermal resistance is

$$\Delta R_X = R_X^t - R_X^0 = R_{int}^t + R_{spr}^t - R_{int}^0 - R_{spr}^0. \quad (3)$$

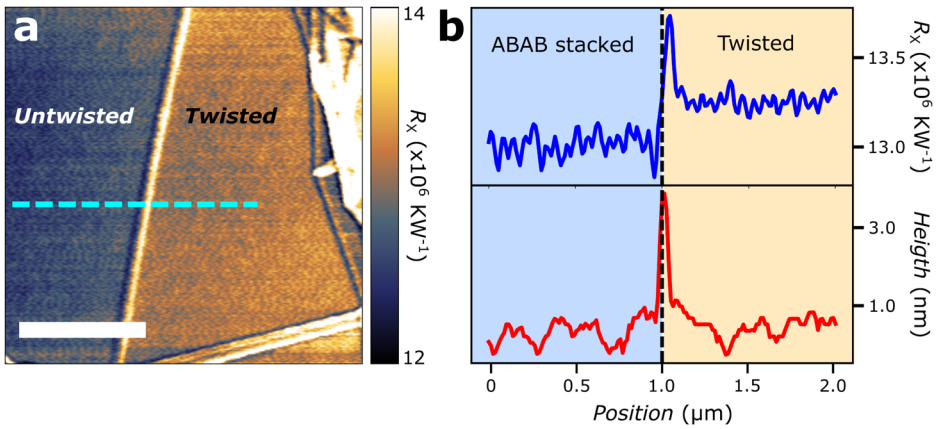

FIG. 3. (a) Thermal resistance map showing higher resistance on the twisted region compared to the non-twisted one. Scale bar is 1 μm. (b) Thermal resistance and topography profiles taken across the transition between the two regions.

The interface resistance (R_{int}) is often a dominant and uncertain factor in SThM measurements. It can be understood as the Kapitza resistance between the phonon systems of the probe and the sample. This resistance is influenced by material properties on both sides of the interface and any surface topography variations. In our case, the probe transitions from untwisted to twisted graphene. As shown in Fig. 3(b), no significant topography change is detected at this boundary.

For graphene–SiO_2 interfaces, reported thermal interface resistivity values range from 5.6×10^{-9} to 7×10^{-8} m^2KW^{-1}.[30,31] Based on our previously estimated contact radius, and assuming that the measured increase ΔR_X is solely due to changes in R_{int}, we estimate that the interface resistivity $r_{int}^{gr-SiO_2}$ increases by approximately 0.5%–3%, depending on the exact contact radius.

Finally, we consider the contribution of the sample thermal spreading resistance (R_{spr}) to the overall measured variation. Given the high thermal conductivity of hBN, we assume it is well thermalized with the underlying silicon oxide substrate. Therefore, the relevant thermal spreading path is defined by the graphene-on-hBN stack, as illustrated in Fig. 2(a). Analytical models for thermal spreading resistance in layered structures[27,28] can be applied here. These models include several key parameters (see the supplementary material for full details): the contact radius a, the in-plane ($k_{\parallel}$) and cross-plane ($k_{\perp}$) thermal conductivities of graphene, the graphene–hBN interface resistivity (r_{int}^{gr-hBN}), and the thermal conductivity of hBN (k_{hBN}).

Next, we consider the in-plane and cross-plane thermal conductivities of the twisted graphene layers. Several studies[32–34] have shown that graphene partially recovers its exceptional thermal transport properties when supported by hBN. The thermal conductivity of suspended single-layer graphene has been measured[35,36] to reach up to 3000 $Wm^{-1}K^{-1}$. When supported on high-quality boron nitride, the reported values[36] approach this suspended limit, typically ranging between 1000 and 2000 $Wm^{-1}K^{-1}$. For the cross-plane direction, bulk graphite exhibits[36] a thermal conductivity of about 5 $Wm^{-1}K^{-1}$.

Using reported values for graphene's in-plane and cross-plane thermal conductivities as inputs, modeling shows that the measured ΔR_X could also be reproduced by a significant reduction in the effective thermal conductivity of the twisted layer, k_{eff}. The effective thermal conductivity describes the spreading of heat away from the tip–sample contact. Following standard treatments of anisotropic media under point heating, k_{eff} is defined as $\sqrt{k_{\parallel} k_{\perp}}$. This geometric mean form accounts for the fact that heat spreading in anisotropic layered systems involves both in-plane and cross-plane transport channels. While the precise magnitude of suppression remains uncertain and may be larger than what is typically reported in Raman-based studies, our result underscores that intrinsic transport changes cannot be excluded and must be considered alongside interfacial effects.

In summary, our estimates show that the measured increase in thermal resistance could arise from a modest variation (0.5%–3%) in tip–sample interface resistivity or from intrinsic conductivity changes within the twisted stack, or a combination of both. While distinguishing between these effects is experimentally challenging, both mechanisms are directly linked to the presence of twist: interlayer reconstruction and local strain can modify phonon transmission across both the graphene–hBN and tip–sample interfaces. The observed and reproducible increase in thermal resistance therefore provides clear experimental evidence that twisting alters the overall heat dissipation pathways at the nanoscale, even if the relative weight of intrinsic and interfacial contributions cannot yet be fully separated.

To better understand the interplay between tip–sample interface resistance and thermal spreading resistance, we now analyze their relative contributions. In Fig. 4, we plot ΔR_X from Eq. (3) as a function of two sets of parameters: (a) tip–sample interface resistivity vs graphene–hBN interface resistivity, and (b) tip–sample resistivity vs effective thermal conductivity of the graphene stack. In both plots, we include a reference line corresponding to the experimentally measured ΔR_X of 0.3×10^6 KW^{-1}.

From Fig. 4(a), it is clear that variations in the graphene–hBN interface resistivity (r_{int}^{gr-hBN}) have a minor impact on the measured ΔR_X. This is attributed to the high in-plane thermal conductivity of the TDBG, which effectively screens the contribution of the underlying interface. Conversely, Fig. 4(b) demonstrates that both a reduction in the effective thermal conductivity of the graphene stack and a modest increase in tip–sample interface resistivity can account for the observed ΔR_X. Our measurements therefore demonstrate that twist alters the local thermal resistance landscape, though the balance between intrinsic and interfacial contributions remains an open question. This broader perspective aligns with prior reports of twist-dependent transport, while also emphasizing the importance of considering interface effects in SThM measurements of twisted systems.

In summary, we have investigated the local thermal transport properties of twisted double bilayer graphene supported on hexagonal

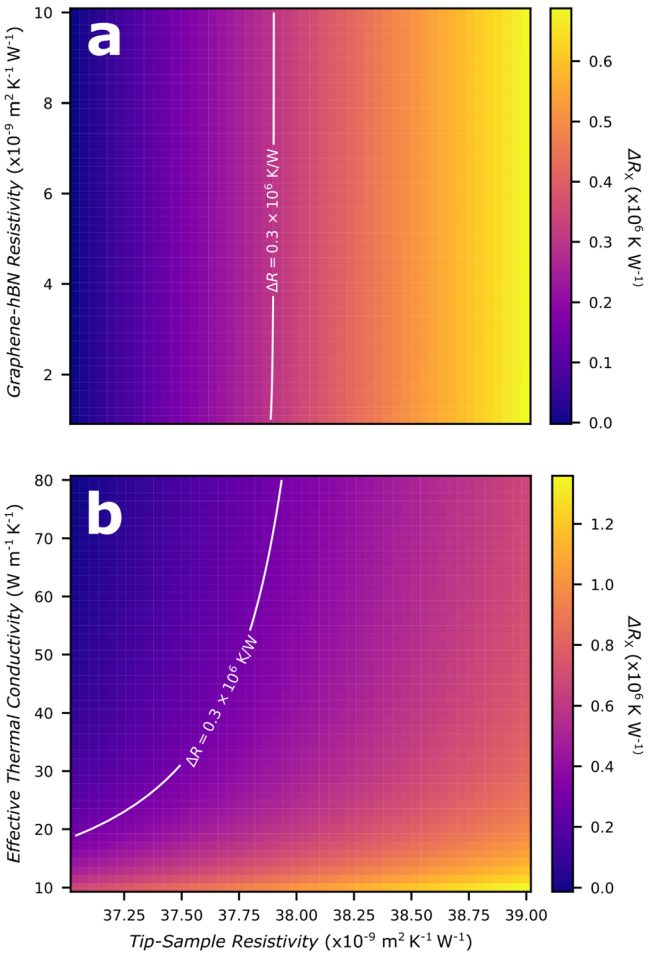

FIG. 4. Thermal resistance variation between twisted and non-twisted regions as a function of graphene–hBN resistivity and tip–sample resistivity (a) and effective thermal conductivity and tip–sample resistivity (b). On both panels, a white line is added to highlight the parameters' set matching the measured variation.

boron nitride using scanning thermal microscopy. Our measurements reveal a measurable increase in thermal resistance in twisted regions compared to untwisted ones. By combining experimental mapping with analytical modeling, we identify possible contributions from both intrinsic thermal conductivity changes and tip–sample interface effects. While distinguishing their relative weight requires further studies across a broader range of twist angles, our results demonstrate that twist modifies the full thermal resistance network of graphene heterostructures. Future studies extending this approach to a wider set of twist angles and multiple samples will be essential to quantify systematic twist-angle trends and verify reproducibility. These results provide direct experimental evidence that twisting graphene layers—while widely used to tune electronic and optical properties—also significantly impacts heat dissipation. Our findings underscore the importance of considering twist angle as a design parameter for future two-dimensional devices, especially in applications where thermal management is critical.

See the supplementary material for additional details on the estimation of SThM lateral resolution and contact radius, reproducibility measurements on multiple twisted regions, and the analytical model used to calculate thermal spreading resistance in anisotropic layered systems.

We acknowledge financial support from the F.R.S.-FNRS of Belgium (Nos. FNRS-CQ-1.C044.21-SMARD, FNRS-CDR-J.0068.21-SMARD, FNRS-MIS-F.4523.22-TopoBrain, FNRS-CR-1.B.463.22-MouleFrits, and FNRS-PDR-T.0029.22-Moiré), from the Federation Wallonie-Bruxelles through the ARC Grant No. 21/26-116 and from the EU (No. ERC-StG-10104144-MOUNTAIN). This project (No. 40007563-CONNECT) has received funding from the FWO and F.R.S.-FNRS under the Excellence of Science (EOS) programme. This work was also partly supported by the FLAG-ERA Grant TATTOOS, through F.R.S.-FNRS PINT-MULTI (Grant No. R 8010.19). We acknowledge the technical support from Bruker UK. The support of the European Union's Horizon 2020 Research Project and Innovation Program–Graphene Flagship Core3 (No. 881603), EPSRC EP/V00767X/1 HiWiN project is fully appreciated. R.R.-P. acknowledges the Flag-Era JTC project TATTOOS (No. R.8010.19) and the Pathfinder project "FLATS" No. 101099139. Sample fabrication was done within the C2N micro nanotechnologies platforms and partly supported by the RENATECH network and the General Council of Essonne. K.W. and T.T. acknowledge support from the JSPS KAKENHI (Grant Nos. 21H05233 and 23H02052), the CREST (No. JPMJCR24A5), JST, and World Premier International Research Center Initiative (WPI), MEXT, Japan.

AUTHOR DECLARATIONS

Conflict of Interest

The authors have no conflicts to disclose.

Author Contributions

Roop Kumar Mech: Data curation (equal); Formal analysis (equal); Investigation (equal); Writing – original draft (equal). **Alessandra Canetta:** Data curation (equal); Investigation (equal); Visualization (equal). **Yubin Huang:** Investigation (equal); Methodology (equal); Validation (equal). **Sergio Gonzalez-Munoz:** Data curation (equal); Investigation (equal). **Khushboo Agarwal:** Investigation (equal); Validation (equal). **Pauline de Crombrugghe:** Investigation (equal). **Yuanzhuo Hong:** Resources (equal). **Sambit Mohapatra:** Investigation (equal); Resources (equal). **Kenji Watanabe:** Investigation (equal); Resources (equal). **Takashi Taniguhi:** Investigation (equal); Resources (equal). **Bernard Nysten:** Data curation (equal); Investigation (equal). **Benoit Hackens:** Funding acquisition (equal); Investigation (equal); Resources (equal). **Rebeca Ribeiro-Palau:** Investigation (equal); Resources (equal); Writing – review & editing (equal). **Oleg Kolosov:** Funding acquisition (equal); Investigation (equal); Methodology (equal). **Jean Spiece:** Conceptualization (equal); Data curation (equal); Formal analysis (equal); Funding acquisition (equal); Investigation (equal); Methodology (equal); Project administration (equal); Supervision (equal); Validation (equal); Visualization (equal); Writing – original draft (equal); Writing – review & editing (equal). **Pascal Gehring:** Conceptualization (equal); Funding acquisition (equal); Investigation (equal); Methodology (equal); Project administration

(equal); Supervision (equal); Validation (equal); Writing – review & editing (equal).

DATA AVAILABILITY

The data that support the findings of this study are available from the corresponding author upon reasonable request.

REFERENCES

[1]A. K. Geim and I. V. Grigorieva, Nature **499**, 419 (2013).
[2]P. Sutter and E. Sutter, iScience **24**, 103050 (2021).
[3]C. Li, P. Zhou, and D. W. Zhang, J. Semicond. **38**, 031005 (2017).
[4]X. Wu, X. Chen, R. Yang, J. Zhan, Y. Ren, and K. Li, Small **18**(15), 2105877 (2022).
[5]F. He, Y. Zhou, Z. Ye, S.-H. Cho, J. Jeong, X. Meng, and Y. Wang, ACS Nano **15**, 5944–5958 (2021).
[6]Y.-N. Ren, Y. Zhang, Y.-W. Liu, and L. He, Chin. Phys. B **29**, 117303 (2020).
[7]S. Carr, D. Massatt, S. Fang, P. Cazeaux, M. Luskin, and E. Kaxiras, Phys. Rev. B **95**, 075420 (2017).
[8]H. D. Saßnick and C. Cocchi, Electron. Struct. **3**, 027001 (2021).
[9]A. Kerelsky, L. J. McGilly, D. M. Kennes, L. Xian, M. Yankowitz, S. Chen, K. Watanabe, T. Taniguchi, J. Hone, C. Dean *et al.*, Nature **572**, 95 (2019).
[10]H. Yoo, R. Engelke, S. Carr *et al.*, Nat. Mater. **18**, 448 (2019).
[11]H. Li, H. Ying, X. Chen, D. L. Nika, A. I. Cocemasov, W. Cai, A. A. Balandin, and S. Chen, Nanoscale **6**, 13402 (2014).
[12]S. Han, X. Nie, S. Gu, W. Liu, L. Chen, H. Ying, L. Wang, Z. Cheng, L. Zhao, and S. Chen, Appl. Phys. Lett. **118**, 193104 (2021).
[13]X. Nie, L. Zhao, S. Deng, Y. Zhang, and Z. Du, Int. J. Heat Mass Transfer **137**, 161 (2019).
[14]M.-H. Wang, Y.-E. Xie, and Y.-P. Chen, Chin. Phys. B **26**, 116503 (2017).
[15]C. Li, B. Debnath, X. Tan, S. Su, K. Xu, S. Ge, M. R. Neupane, and R. K. Lake, Carbon **138**, 451 (2018).
[16]L. P. Krisna, T. Kawakami, and M. Koshino, J. Phys. Soc. Jpn. **94**, 044602 (2025).
[17]H. Feng, B. Liu, and Z.-X. Guo, Phys. Rev. B **108**, L241405 (2023).
[18]W. Ouyang, H. Qin, M. Urbakh, and O. Hod, Nano Lett. **20**, 7513 (2020).
[19]Y. Li, X. Wang, D. Tang, X. Wang, K. Watanabe, T. Taniguchi, D. R. Gamelin, D. H. Cobden, M. Yankowitz, X. Xu, and J. Li, Adv. Mater. **33**, 2105879 (2021).
[20]H. Li, Z. Ying, B. Lyu, A. Deng, L. Wang, T. Taniguchi, K. Watanabe, and Z. Shi, Nano Lett. **18**, 8011–8015 (2018).
[21]A. Gadelha, D. Ohlberg, F. Santana, E. Silva, J. Lemos, V. Ornelas, D. Miranda, R. Nadas, K. Watanabe, T. Taniguchi, C. Rabelo, P. Venezuela, G. Medeiros-Ribeiro, A. Jorio, L. Cançado, and L. Campos, ACS Appl. Nano Mater. **4**, 1858 (2021).
[22]K. Kim, A. DaSilva, S. Huang, B. Fallahazad, S. Larentis, T. Taniguchi, K. Watanabe, B. J. LeRoy, A. H. MacDonald, and E. Tutuc, Proc. Natl. Acad. Sci. U. S. A. **114**, 3364 (2017).
[23]L. McGilly, A. Kerelsky, N. Finney, K. Shapovalov, E.-M. Shih, A. Ghiotto, Y. Zeng, S. Moore, W. Wu, Y. Bai, K. Watanabe, T. Taniguchi, M. Stengel, L. Zhou, J. Hone, X. Zhu, D. Basov, C. Dean, C. Dreyer, and A. Pasupathy, Nat. Nanotechnol. **15**, 580–584 (2020).
[24]A. Canetta, S. Gonzalez-Munoz, V.-H. Nguyen, K. Agarwal, P. D. C. de Picquendaele, Y. Hong, S. Mohapatra, K. Watanabe, T. Taniguchi, B. Nysten *et al.*, Nanoscale **15**, 8134 (2023).
[25]S. Hong, J. Appl. Phys. **129**, 051101 (2021).
[26]A. Kerelsky, C. Rubio-Verdú, L. Xian, D. M. Kennes, D. Halbertal, N. Finney, L. Song, S. Turkel, L. Wang, K. Watanabe, T. Taniguchi, J. Hone, C. Dean, D. N. Basov, A. Rubio, and A. N. Pasupathy, Proc. Natl. Acad. Sci. **118**, e2017366118 (2021).
[27]J. Spiece, C. Evangeli, K. Lulla, A. Robson, B. Robinson, and O. Kolosov, J. Appl. Phys. **124**, 015101 (2018).
[28]J. Spiece, S. Sangtarash, M. Mucientes, A. J. Molina-Mendoza, K. Lulla, T. Mueller, O. Kolosov, H. Sadeghi, and C. Evangeli, Nanoscale **14**, 2593 (2022).
[29]S. Gonzalez-Munoz, K. Agarwal, E. G. Castanon, Z. R. Kudrynskyi, Z. D. Kovalyuk, J. Spièce, O. Kazakova, A. Patanè, and O. V. Kolosov, Adv. Mater. Interfaces **10**, 2300081 (2023).
[30]Z. Chen, W. Jang, W. Bao, C. Lau, and C. Dames, Appl. Phys. Lett. **95**, 161910 (2009).
[31]P. Yasaei, C. J. Foss, K. Karis, A. Behranginia, A. I. El-Ghandour, A. Fathizadeh, J. Olivares, A. K. Majee, C. D. Foster, F. Khalili-Araghi *et al.*, Adv. Mater. Interfaces **4**, 1700334 (2017).
[32]X. Wang, T. Huang, and S. Lu, Appl. Phys. Express **6**, 075202 (2013).
[33]Z. Zhang, S. Hu, J. Chen, and B. Li, Nanotechnology **28**, 225704 (2017).
[34]S. Karak, S. Paul, D. Negi, B. Poojitha, S. K. Srivastav, A. Das, and S. Saha, ACS Appl. Nano Mater. **4**, 1951 (2021).
[35]A. A. Balandin, S. Ghosh, W. Bao, I. Calizo, D. Teweldebrhan, F. Miao, and C. N. Lau, Nano Lett. **8**, 902 (2008).
[36]E. Pop, V. Varshney, and A. K. Roy, MRS Bull. **37**, 1273 (2012).